Abinitio determination of crystal structures of the thermoelectric material MgAgSb

Melanie J. Kirkham, Antonio M. dos Santos, Claudia J. Rawn, Edgar Lara-Curzio, Jeff W. Sharp, and Alan J. Thompson

Phys. Rev. B **85**, 144120 — Published 27 April 2012

DOI: 10.1103/PhysRevB.85.144120

Ab-initio determination of crystal structures of the thermoelectric material MgAgSb

Melanie J. Kirkham*[1], Antonio M. dos Santos[2], Claudia J. Rawn[1,3], Edgar Lara-Curzio[1], Jeff W. Sharp[4] and Alan J. Thompson[4]

[1] Materials Science and Technology Division, Oak Ridge National Laboratory, Oak Ridge, TN 37831

[2] Quantum Condensed Matter Division, Oak Ridge National Laboratory, Oak Ridge, TN 37831

[3] Department of Materials Science and Engineering, University of Tennessee, Knoxville, TN 37996

[4] Marlow Industries, Inc. (subsidiary of II-VI Inc.), Dallas, TX 75238

(Dated: February 17, 2012)

ABSTRACT

Materials with the half-Heusler structure possess interesting electrical and magnetic properties, including potential for thermoelectric applications. MgAgSb is compositionally and structurally related to many half-Heusler materials, but has not been extensively studied. This work presents the high-temperature X-ray diffraction analysis of MgAgSb between 27 and 420°C, complemented with thermoelectric property measurements. MgAgSb is found to exist in three different crystal structures in this temperature region, taking the half-Heusler structure at high temperatures, a Cu_2Sb-related structure at intermediate temperatures, and a previously unreported tetragonal structure at room temperature. All three structures are related by a distorted Mg-Sb rocksalt-type sublattice, differing primarily in the Ag location among the available tetrahedral sites. Transition temperatures between the three phases correlate well with discontinuities in the Seebeck coefficient and electrical conductivity; the best performance occurs with the novel room temperature phase. For application of MgAgSb as a thermoelectric material, it may be desirable to develop methods to stabilize the room temperature phase at higher temperatures.

PACS numbers: 61.66.-Fn, 84.60.Rb, 61.05.cp

I. INTRODUCTION AND BACKGROUND

Heusler and half-Heusler materials are a fascinating class of intermetallic compounds with crystal structures related to fluorite. The general chemical formulas are X_2YZ and XYZ, respectively, where usually X, the most electropositive element, is an alkali, alkali earth, early transition metal or rare earth element; Y is a late transition metal; and Z, the most electronegative element, is from groups 13, 14 or 15. Compounds in this class have been shown to possess interesting electrical and magnetic properties, including superconductivity and spintronic applications[1]. Among other possible areas, half-Heusler compounds have been investigated for thermoelectric applications[1].

Thermoelectric generators, which convert a temperature differential into usable electrical power, hold great promise for improving energy efficiency by harvesting waste heat from vehicles, industrial processes, etc. However, the application of thermoelectric generators is currently hampered by their low efficiency, which is a function of the temperature difference between the hot and cold side and a dimensionless figure-of-merit, ZT, a property of the thermoelectric materials. Thermoelectric generators have found use in some specialized applications, such as radioisotope thermoelectric generators (RTGs) for powering deep-space probes, where the large temperature difference between the radioisotope and the cold of space compensates for the low ZT. For non-space commercial applications, thermoelectric materials with higher figures-of-merit need to be developed[2].

The thermoelectric properties of Half-Heusler compounds have been studied[3,4]. One benefit is that the thermoelectric properties of half-Heusler compounds can be tailored by substitution on each of the three atomic positions. The half-Heusler crystal structure consists of three interpenetrating face-centered cubic (FCC) lattices, forming a rocksalt-type lattice with half of the tetrahedral interstices filled. Of four special positions in the space group $F\bar{4}3m$, one sits empty, as outlined in Table I. Two variations of the crystal structure exist, depending on which atoms fill which sites. Assuming the empty site is 4d, the more common structural variation (II, as notated Graf, Felser and Parkin[1]) has the most and least electronegative elements (X and Z) sitting on the 4a and 4b sites, and the transition metal (Y) filling the 4c site. Examples include MgCuBi, MgCuSb[5,6], ZnAgAs[7], MgNiBi, MnCuSb, MgNiBi and MgNiSb[8]. Less commonly (variation I), the two more electropositive elements (X and Y) sit on the 4a and 4b sites, and the 4c site is filled by the most electronegative element (Z). Examples include MgAgAs[5] and NaZnAs[7].

Table I. Filling of atomic positions in two variations of the half-Heusler structure, XYZ, using the nomenclature proposed by Graf, Felser and Parkin[1], where X and Z are the least and most electronegative elements, respectively, and Y is a late transition metal.

Wyckoff	Atomic position			Atom type	
symbol	x	y	z	Var. I	Var. II
4a	0	0	0	X	Z
4b	½	½	½	Y	X
4c	¼	¼	¼	Z	Y
4d	¾	¾	¾	empty	empty

Given the fact that many related compositions take the half-Heusler crystal structure, it is reasonable to expect that MgAgSb would follow suit; however this phase has not been extensively studied, in particular with regards to its crystal structure. Nowotny and Sibert in 1941 published an X-ray diffraction study in which they reported that the crystal structure of MgAgSb is related to that of MgCuAs, likely with reduced symmetry[5]. MgCuAs does not

take the half-Heusler structure; instead it is related to the tetragonal Cu_2Sb crystal. However, in a later study of the Mg-Ag-Sb phase diagram, Frost and Raynor[9] reported that the MgAgSb ternary had a fluorite structure, as in the half-Heusler structure. The purpose of this research is to study the crystal structure of MgAgSb at both ambient and elevated temperatures and to investigate its thermoelectric properties as a function of temperature.

II. EXPERIMENTAL METHODS

MgAgSb samples were synthesized by compounding elemental powders in <50 ppm O_2 ,N_2 atmosphere. The compounded elements were sealed in an evacuated, flame dried quartz tube, heated to 975°C for 4 hours, and then air-quenched. The resulting charge was ground to <45μm, hot-pressed to approximately 98 percent of theoretical density and annealed at 300°C for seven days. The consolidation was performed at 350°C under a 5600kgf load in a N_2 atmosphere. The consolidated samples were ground a final time before diffraction analysis.

Non-ambient x-ray diffraction (XRD) data were collected on an X'Pert Pro diffractometer (PANalytical B.V., Almelo, The Netherlands) with Cu Kα radiation and a position-sensitive detector. The diffractometer was in parafocusing geometry, with 0.04 rad. Soller slits and ¼° divergence and receiving slits. The powder samples were heated with an XRK900 reaction chamber (Anton Paar GmbH, Graz, Austria) under the flow of N_2 to prevent oxidation. XRD scans were collected every 30°C from 30°C to 420°C, with a heating rate between steps of 30°C/min. A hold for 20 min at each step provided time for the XRD scan from 10 to 90° 2θ. The furnace temperature was held for 1 min before each scan for temperature equilibration. XRD data were collected over two full cycles on heating and cooling. Additionally, another XRD scan was collected from the recovered sample, outside the furnace, with an increased range (5 to 140° 2θ) and scan time (14.5 hr). Guided by the first set of results, a second set of high-temperature X-ray diffraction (HTXRD) data was collected with a smaller temperature step (5°C) between scans, with a one hour hold for data collection at each step, preceded by a 2 min. wait for temperature equilibrium, and a heating rate of 60°/min between steps. The XRD spectra were analyzed with the HighScore Plus computer program (version 3.0.3; PANalytical B.V., Almelo, The Netherlands).

For *ab-initio* structural solution, the unit cell parameters were obtained using TREOR[10] as implemented in PowderX[11] and HighScore, and space groups were suggested by CheckCell[12]. The structure was determined concurrently with a real-space Monte-Carlo search using a parallel tempering algorithm implemented in FoX[13] and with charge flipping analysis using Superflip[14] as implemented in HighScore. Crystal structures were visualized with Vesta[15]. The solved crystal structures were refined using the Rietveld method as implemented in HighScore, using a pseudo-Voight profile function with the Finger-Cox-Jephcoat[16] asymmetry correction. The thermal parameters were found to be highly correlated, and therefore were constrained to be equal. Additionally, the occupancies refined to values not statistically significantly different than 1, and were therefore fixed at that value.

The Seebeck coefficient (S) and electrical resistivity (ρ) of MgAgSb were measured between 30 and 410°C, at 20° intervals, using an ULVAC, Model ZEM-3 M8. The sample dimensions were 2×2×12 mm^3. The thermoelectric power factor (PF) was determined from the Seebeck coefficient, S, and resistivity, ρ, using the equation $PF = S^2/\rho = S^2\sigma$. The thermal conductivity (λ) was obtained by measuring the thermal diffusivity (κ) and specific heat per unit volume (C_V), and calculated according to the equation $\lambda = \kappa^* C_V$. The thermal diffusivity was measured on a ∅12.7 mm × 1mm thick sample using an Anter FL5000 graphite furnace, 20-2500°C, YAG laser, InSb detector, ASTM 1461system. The specific heat was measured on a 5×5×1 mm^3 specimen using a Netzsch DSC 404C (RT-1400°C) system.

III. NON-AMBIENT X-RAY DIFFRACTION

Non-ambient X-ray diffraction patterns are shown in Fig. 1. Several phase transitions are observed during the two heating/cooling cycles. On heating, the initial room-temperature phase (which we will refer to as α-MgAgSb) is stable up to 290°C, above which it transforms to an intermediate phase (β-MgAgSb), a process completed before the scan at 315°C. (The precise transition temperatures were determined from HTXRD data collected in increments of 5°C.) The intermediate phase, β-MgAgSb, is stable up to 360°C, above which it transforms to a high-temperature phase (γ-MgAgSb), a process completed before the scan at 395°C. The high-temperature phase, γ-MgAgSb, is stable up to the maximum temperature reached during the experiment, 420°C. These phases are not reported for this composition in the powder diffraction databases, and therefore the structures were solved *ab initio* as discussed below. Small amounts of elemental antimony and dyscrasite (Ag_3Sb) secondary phases present in the initial sample (6.5±0.2 and 5.5±0.2mol%, respectively) grow during the first heating cycle to 14.4±0.4 and 19.4±0.4mol%, respectively, after which the amounts of the secondary phases stay approximately constant. Representative scans collected at 30, 330 and 420°C are shown in Fig. 2.

On cooling, a somewhat different behavior of the major phase is observed. Only γ-MgAgSb, the high-temperature phase, is present down to around 210°C, where it partially transforms to α-MgAgSb, the room-temperature phase, skipping β-MgAgSb, the intermediate phase. The γ-MgAgSb phase persists to some extent all the way down to the minimum temperature of 30°C. This supercooling and persistence of γ-MgAgSb points to its stability and a possible kinetics effect; however, this is outside the scope of this report, which will focus on the three phases as observed during heating.

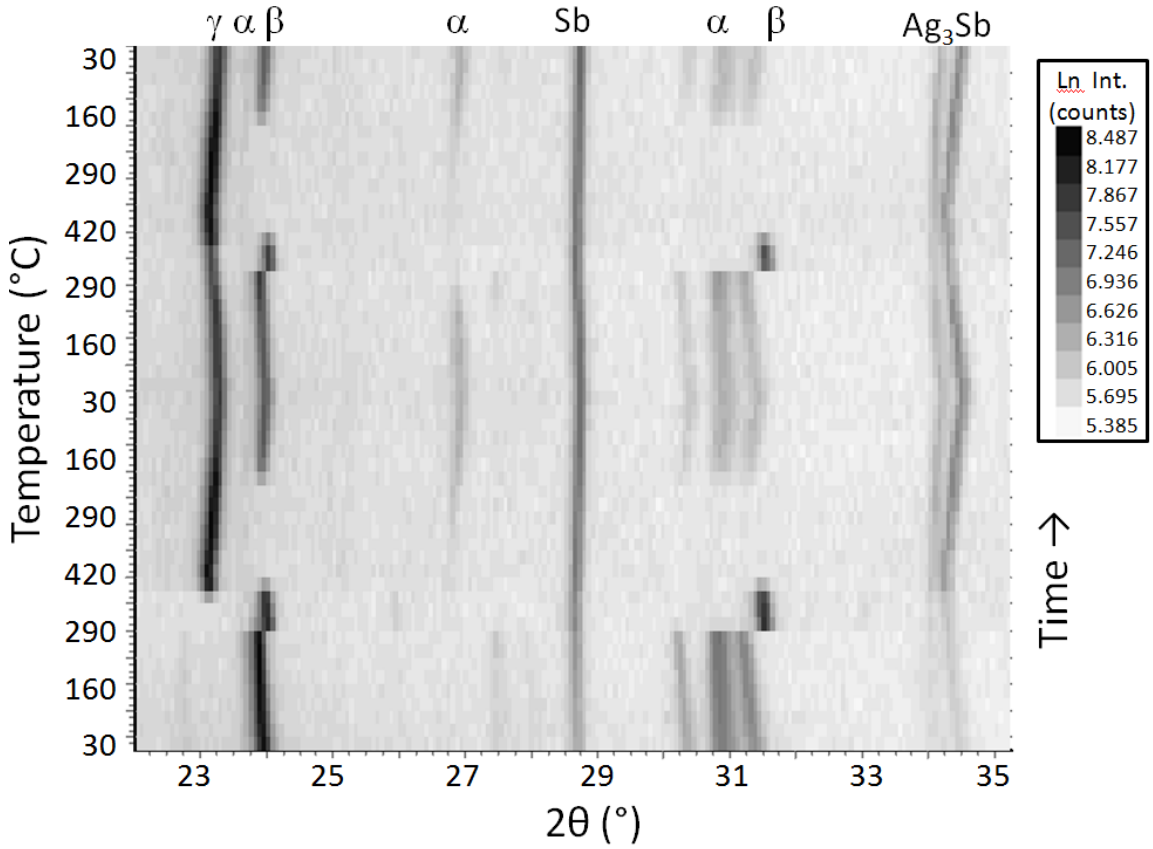

FIG. 1. Detail of non-ambient X-ray diffraction data collected on MgAgSb over two cycles of heating and cooling between 30 and 420°C, showing the room-temperature, intermediate and high-temperature MgAgSb phases (α-, β- and γ-MgAgSb, respectively) and secondary phases of Sb and Ag_3Sb.

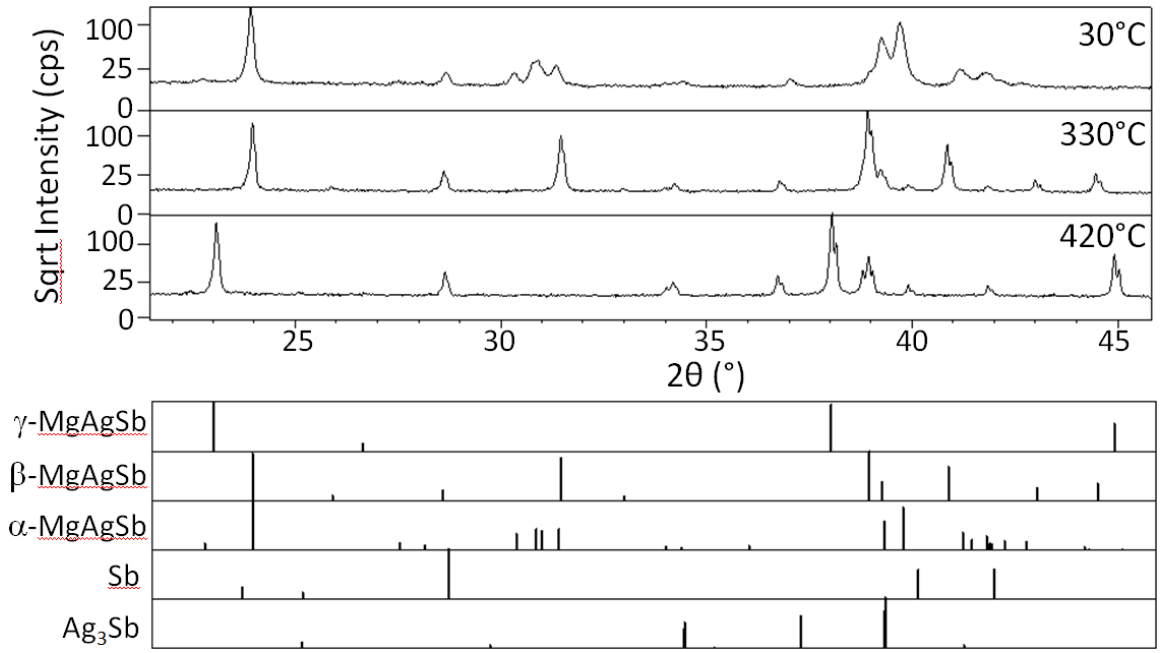

FIG. 2. Representative HTXRD scans collected at 30°C (top in blue), 330°C (middle in green) and 420°C (bottom in red), along with the peak positions for the room-temperature, intermediate and high-temperature MgAgSb phases (α-, β- and γ-MgAgSb, respectively) and the two secondary phases of Sb and Ag_3Sb underneath.

IV. CRYSTAL STRUCTURES

A. High-temperature MgAgSb phase

A diffraction pattern of the high-temperature γ-MgAgSb phase collected at 420°C was indexed and determined to be cubic, with space group $F\bar{4}3m$ (216), and Z=4. The refined structural parameters are given in Table II. The crystal structure is, in fact, identical to the half-Heusler structure. As discussed above, the half-Heusler structure exists in two variations, depending on the atomic arrangements, i.e. which atoms form the rocksalt sublattice. For this material, the most and least electronegative atoms (antimony and magnesium, respectively) form a rocksalt-type sublattice. This is the more common version of the half-Heusler structure, isostructural with MgCuSb[5,6]. The silver atoms fill half of the tetrahedral interstices, alternating between filled and empty sites. An examination of the crystal structure, shown in Fig. 3, shows that each silver atom is surrounded by four magnesium and four antimony atoms, forming a Mg-Sb cube.

Table II. Refined structural parameters of the room-temperature, intermediate and high-temperature phases (α-, β- and γ-MgAgSb, respectively). Estimated standard deviations of refined values are given in parentheses; these values are known to be underestimates of the true deviations, providing however a measure of the minimum uncertainty[17]. The values a_c and c_c are the rocksalt sublattice parameters, derived from the tetragonal lattice parameters, as discussed in the text.

Phase	γ-MgAgSb	β-MgAgSb	α-MgAgSb		
Temperature (°C)	420	330	room		
Space group	F$\bar{4}$3m (216)	P4/nmm (129)	I$\bar{4}$c2 (120)		
a (Å)	6.7004(1)	4.4199(1)	9.1761(4)		
c (Å)	--	6.8896(2)	12.6960(7)		
a_c (Å)	--	6.2507	6.4884		
c_c (Å)	--	6.8896	6.3480		
c_c/a_c	1	1.1022	0.9783		
Z	4	2	16		
Theor. density (g/cm^3)	5.61	6.26	6.31		
Mg Wyckoff site	4b	2c	16i		
x	½	¼	-0.036(3)		
y	½	¼	0.296(2)		
z	½	0.333(1)	0.096(1)		
Ag Wyckoff site	4c	2a	8e	4a	4b
x	¼	¾	0.2244(7)	0	0
y	¼	¼	0.2244(7)	0	0
z	¼	0	¼	¼	0
Sb Wyckoff site	4a	2c	16i		
x	0	¼	0.2363(5)		
y	0	¼	0.4749(7)		
z	0	0.7292(4)	0.1203(4)		
R_{exp}	5.882	5.808	1.645		
R_{wp}	7.622	7.539	4.633		
χ^2	1.679	1.685	7.930		
# refined parameters	22	22	38		

# reflections	109	124	484

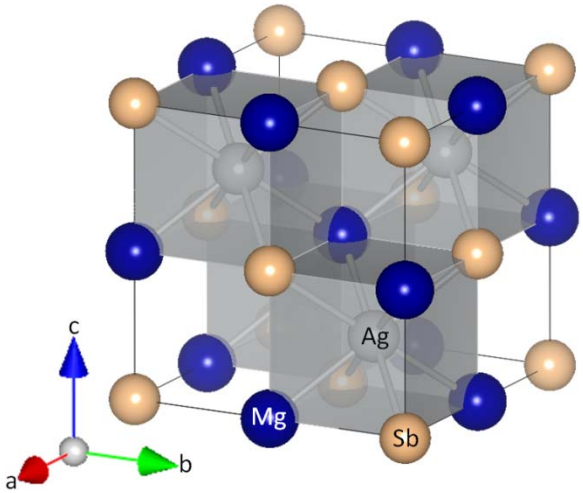

FIG. 3. (Color online) Crystal structure of the high-temperature γ-MgAgSb phase, with the Mg shown in dark blue, the Sb in light tan and the Ag in silver inside the polyhedra.

B. Intermediate MgAgSb phase

A diffraction pattern of the intermediate β-MgAgSb phase collected at 330°C was indexed and determined to be tetragonal, with space group P4/nmm (129), and Z=2. The refined parameters are given in Table II, and the structure is displayed in Fig. 4. Although the crystal structure appears at first glance to be quite different from the γ-MgAgSb half-Heusler structure, a closer examination reveals similarities. In the intermediate phase, the Mg and Sb atoms form a rocksalt lattice, as in the high temperature phase, albeit a rather distorted one. The rocksalt lattice and tetragonal unit cell lattice are related by a 45° rotation about the *c*-axis. The lattice parameters of the distorted rocksalt sublattice (a_c and c_c) can be calculated from the tetragonal lattice parameters (a_t and c_t) thusly: $a_c = a_t * \sqrt{2}$ and $c_c = c_t$. The Ag atoms fill half of the distorted Mg-Sb pseudo-cubes. This structure is related to the Cu_2Sb structure[6,18], with silver and magnesium each replacing one of the two copper sites. Few structural analogs of this phase have been reported; MgCuAs has been reported to have this structure[5], although more recent results suggest that it is actually a related orthorhombic structure[6].

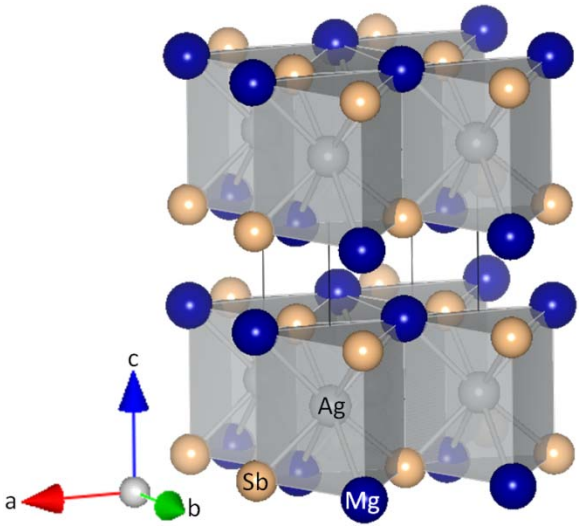

FIG. 4. (Color online) Crystal structure of the intermediate β-MgAgSb phase, drawn to include atoms outside the unit cell in order to emphasize the distorted rocksalt lattice of Mg and Sb atoms, with the Mg shown in dark blue, the Sb in light tan and the Ag in silver inside the polyhedra.

C. Room-temperature MgAgSb phase

A diffraction pattern of the room-temperature α-MgAgSb phase collected at room temperature was indexed and determined to also be tetragonal, with space $I\bar{4}c2$ (120), and Z=16. The structure was refined using the longer, slower XRD scan collected after heating; the better quality data helped remedy difficulties due to the complexity of the structure and the presence of other phases. The refined parameters are given in Table II, and the structure is displayed in Fig. 5. Similar to the intermediate phase, the room-temperature phase consists of a distorted Mg-Sb rocksalt lattice, rotated by 45° about the *c*-axis, with half of the Mg-Sb pseudo-cubes filled with Ag. The unit cell of the room temperature phase is doubled along both axes to accommodate a different ordering of the Ag atoms, as will be discussed below. The lattice parameters of the distorted rocksalt sublattice (a_c and c_c) can be calculated from the tetragonal lattice parameters (a_t and c_t), thusly: $a_c = a_t/\sqrt{2}$ and $c_c = c_t/2$. No structural analogs of this phase were found in the literature.

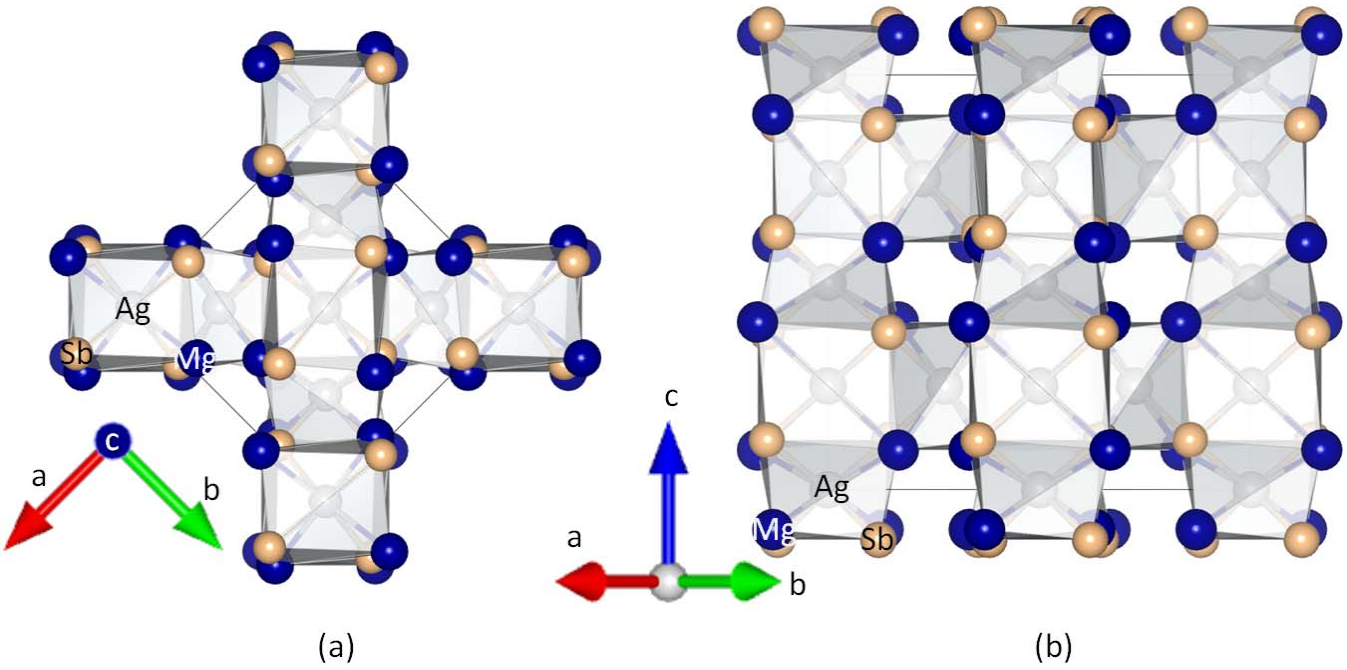

FIG. 5. (Color online) Crystal structure of the room-temperature α-MgAgSb phase, looking along the (a) <001> and (b) <110> directions, drawn to include atoms outside the unit cell in order to emphasize the distorted rocksalt lattice of Mg and Sb atoms, with the Mg shown in dark blue, the Sb in light tan and the Ag in silver inside the polyhedra.

These three crystal structures of MgAgSb, which appear rather different at first, actually have certain similarities. As mentioned earlier, all three structures contain an Mg-Sb rocksalt lattice; although in the intermediate and room-temperature phases, this lattice is distorted. In all three structures, half of the Mg-Sb cubes are filled with silver atoms. The primary difference between the three MgAgSb structures lies in the pattern of filling of the Mg-Sb cubes with Ag. In γ-MgAgSb with the half-Heusler structure, alternating sites are filled in a three-dimensional arrangement. In β-MgAgSb with a Cu_2Sb-type structure, there are alternating fully-occupied and fully-empty planes perpendicular to the *c*-axis, a two-dimensional arrangement. In α-MgAgSb, the filled sites form one-dimensional chains, running in all three primary directions.

V. THERMAL EXPANSION AND THERMOELECTRIC PROPERTIES

As discussed above, the lattice parameters of the Mg-Sb rocksalt sublattice can be determined from the lattice parameters of the full cells, and their values are plotted in Fig. 6 as a function of temperature, revealing three observations. First, the tetragonal distortion is significantly larger (~12%) for the intermediate β phase than for the room temperature α phase. This can be understood by recognizing that the Ag ion distribution is essentially three dimensional in the α phase and layered in the β phase, thereby increasing the anisotropic character of the tetragonal structure. Second, the average sublattice parameters of both α- and β-MgAgSb phases are smaller than the lattice parameter for cubic γ-MgAgSB. The symmetry of the γ phase requires that the empty Mg-Sb cubes be

as large as the filled ones, resulting in a larger cell, as compared to the β- and α-MgAgSb phases, in which the empty Mg-Sb cubes are significantly smaller than the filled ones.

Third, the thermal expansion of the room-temperature α phase becomes non-linear above 300°C. The *a*-axis of the rocksalt sublattice increases and the *c*-axis decreases, leading to increasing tetragonal distortion. This increasing anisotropy occurs as the phase approaches the transformation to the more anisotropic β phase. The lattice coefficients of thermal expansion (CTEs) were determined from the measured lattice parameters of the three MgAgSb phases (Table III). For the room-temperature α phase, only data up to 300°C, the onset of non-linearity, were included. For the β-MgAgSb phase, CTEs were referenced to the cell at 300°C, since phase does not exist at room temperature. The thermal expansion of the room-temperature α phase is significantly anisotropic, with the CTE for the *c*-axis being approximately twice that for the *a*-axis. The CTE for the β phase is more isotropic and similar to that for the γ phase.

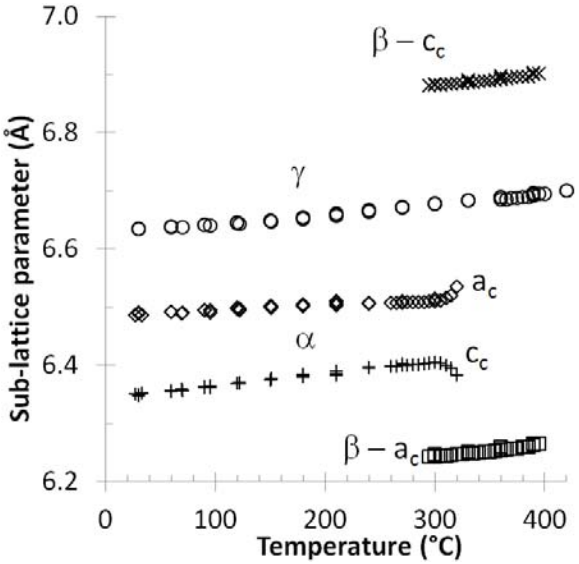

FIG. 6. Lattice parameters of the Mg-Sb rocksalt sublattice of the three MgAgSb phases, determined for the α- and β-phases from the tetragonal lattice parameters, as a function of temperature. Error bars, based on estimated standard deviations, are smaller than the symbols.

Table III. Lattice coefficients of thermal expansion (CTEs) in the *a*- and *c*-axes and the unit cell volume determined from the measured lattice parameters of the three MgAgSb phases. Standard deviations are given in parentheses.

	Range	Lattice CTE (10^{-6}/K)		
Phase	(°C)	*a*	*c*	Vol.
α	27-300	15(2)	33(2)	63(5)
β	300-395	27(5)	24(6)	79(16)
γ	27-420	21(4)	-	63(13)

These structural transformations of MgAgSb correlate with observed changes in thermoelectric properties, namely the Seebeck coefficient (S) and electrical conductivity (σ), as shown in Fig. 7, and the thermal conductivity (λ), as shown in Fig. 8. Discontinuous changes in S and σ can be seen around 300 and 390°C, approximately the same temperatures as the phase transitions observed in the non-ambient X-ray diffraction analysis. The thermoelectric power factor ($S^2\sigma$) is highest in the room-temperature α phase, reaching a maximum of 18 μW/cm·K^2 at 290°C. The intermediate β phase, which contains the Ag planes, has a higher electrical conductivity, but a much lower Seebeck coefficient, leading to a low power factor, around 2 μW/cm·K^2. In the high-temperature γ phase, the Seebeck coefficient returns to higher values, but the electrical conductivity is significantly lower, again leading to a low power factor, around 4 μW/cm·K^2. Preliminary investigations of the thermal conductivity from room temperature up to 202°C indicate that it is quite low, approaching 1.1 W/m·K at room temperature, as shown in Fig. 8. The large unit cell of the room-temperature α phase contributes to its low lattice thermal conductivity[19]. Combining the power factor and thermal conductivity, the maximum ZT reaches a value of ~0.56 at temperatures around 150 to 170°C, as seen in Fig. 8. This is promising since the material has not yet been optimized and therefore further improvements in ZT should be possible.

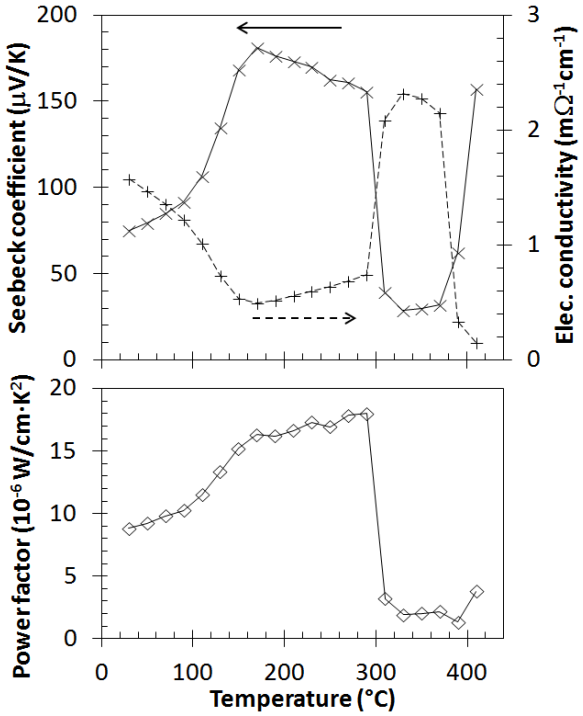

FIG. 7. Seebeck coefficient, S, and electrical conductivity, σ, (top) and thermoelectric power factor, $S^2\sigma$, (bottom) of MgAgSb between 30 and 410°C.

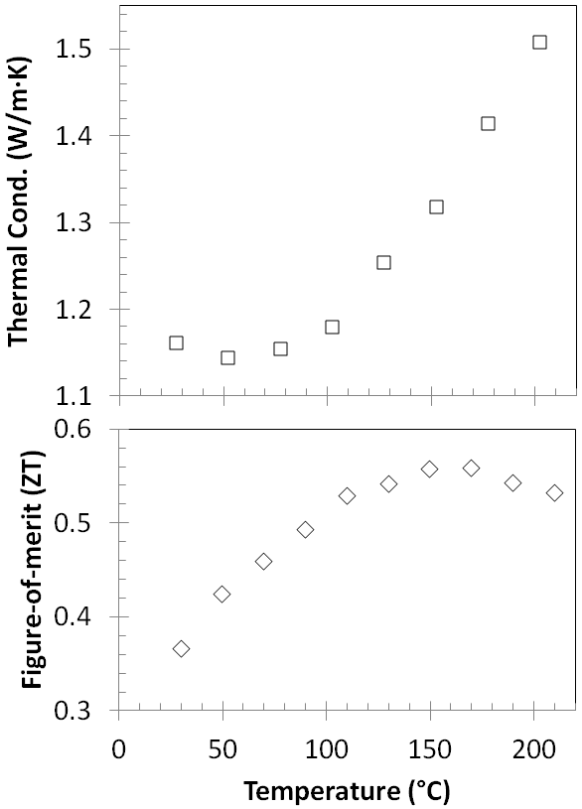

FIG. 8. Thermal conductivity, λ, (top) and thermoelectric figure-of-merit, ZT, (bottom) of MgAgSb.

VI. SUMMARY

In this work, the crystal structure of MgAgSb, a potential thermoelectric material, was investigated in the temperature range 30-420°C. MgAgSb exists in three different structures in this temperature range. The high-temperature γ phase, present above ~360°C, is cubic (space group $F\bar{4}3m$), with the half-Heusler structure, as has been previously reported for many analogous phases. The intermediate β phase, present between ~300 and 360°C, is tetragonal (space group P4/nmm), with a Cu_2Sb-type structure, similar to MgCuAs. The room-temperature α phase is also tetragonal (space group $I\bar{4}c2$), although with a larger unit cell. In all three phases, the Mg and Sb atoms form a rocksalt-type structure, distorted for the intermediate and room temperature phases, while the Ag atoms fill half of the Mg-Sb cubes, with different filling patterns for each phase. The Seebeck coefficient and electrical conductivity undergo discontinuous changes around the same temperatures as the phase transitions, with the maximum thermoelectric power factor 18 $\mu W/cm \cdot K^2$ being observed in the room-temperature phase at 290°C. For application as a thermoelectric material, it may be desirable to develop methods to stabilize the room temperature phase at higher temperatures.

ACKNOWLEDGEMENTS

The authors wish to thank Andrew Payzant at Oak Ridge National Laboratory for helpful discussions. This research through the Oak Ridge National Laboratory's High Temperature Materials Laboratory User Program was sponsored by the U. S. Department of Energy, Office of Energy Efficiency and Renewable Energy, Vehicle Technologies Program and by the Center on Revolutionary Materials for Solid State Energy Conversion, an Energy Frontier Research Center funded by the U. S. Department of Energy, Office of Basic Energy Sciences under Award Number DE-SC0001054. ORNL/NSSD is managed by UT-Battelle, LLC, for the U.S. Department of Energy under contract DE-AC05-00OR22725.

*Author to whom correspondence should be addressed: kirkhammj@ornl.gov; (865)574-6538.

[1] T. Graf, C. Felser, and S.S.P. Parkin, Prog. Solid State Chem. **39**, 1 (2011).
[2] L.E. Bell, Science **321**, 1457 (2008).
[3] G.S. Nolas, J. Poon, and M. Kanatzidis, MRS Bull. **31**, 199 (2006).
[4] J. Poon, D. Wu, S. Zhu, W. Xie, T. Tritt, P. Thomas, and R. Venkatasubramanian, J. Mater. Res. **26**, 2795 (2011).
[5] H. Nowotny and W. Sibert, Z. Metallkd. **33**, 391 (1941).
[6] J. Nuss and M. Jansen, Z. Anorg. Allg. Chem. **628**, 1152 (2002).
[7] H. Nowotny and B. Glatzl, Monatsh. Chem. **82**, 720 (1951).
[8] H. Nowotny and B. Glatzl, Monatsh. Chem. **83**, 237 (1952).
[9] B.R.T. Frost and G.V. Raynor, Proc. R. Soc. Lon. A **203**, 132 (1950).
[10] P.E. Werner, L. Eriksson, and M. Westdahl, J. Appl. Cryst. **18**, 367 (1985).
[11] C.J. Dong, J. Appl. Cryst. **32**, 838 (1999).
[12] J. Laugier and B. Bochu, computer code *CHECKCELL*, Collaborative Computational Project Number 14 (CCP14), Laboratoire des Matériaux et du Génie Physique de l'Ecole Supérieure de Physique de Grenoble (INPG), France, 2000.
[13] V. Favre-Nicolin and R. Černý, J. Appl. Cryst. **35**, 734 (2002).
[14] L. Palatinus and G. Chapuis, J. Appl. Cryst. **40**, 786 (2007).
[15] K. Momma and F. Izumi, J. Appl. Cryst. **41**, 653 (2008).

[16] L.W. Finger, D.E. Cox, and A.P. Jephcoat, J. Appl. Cryst. **27**, 892 (1994).
[17] B.H. Toby, Powder Diffr. **21**, 67 (2006).
[18] W.B. Pearson, Z. Kristallogr. **171**, 23 (1985).
[19] G.A. Slack, Solid State Phys. **34**, 1 (1979).